

Estimating porosity and permeability using Digital Image Analysis (DIA) technique for highly porous sandstones

Bassem S. Nabawy

Received: 9 July 2012 / Accepted: 21 December 2012 / Published online: 5 January 2013
© Saudi Society for Geosciences 2013

Abstract In the present study, 12 theoretical models have been introduced for studying the effect of the grain size and shape on the intergranular porosity, ϕ . From the first eight models, it is stated that the grain size has no effect on the intergranular porosity, but it is declared that the smaller the grain size means the smaller the interstitial pore spaces and therefore, the less the ability of the pore spaces to receive finer sediments, then the higher the porosity. On the other hand, studying the present models revealed that the total intergranular porosity decreases when increasing the grain elongation ' E ' (the length of the grain/the diameter of the grain) as a shape anisotropy parameter. A new equation has been introduced relating the total pore volume to the grain shape/elongation.

$$\phi = 26.188 E^{-1} + 21.431$$

The grain sorting of the present models has been studied by adding another group of grains of the critical grain size of occupation inside the pore spaces; the pore volume decreases by about 41.0 % of the total porosity. To check the applicability of the proposed equation, 46 samples of highly porous sandstone have been selected from different places in Egypt and studied petrographically, and their total pore volume have been measured using Digital Image Analysis (DIA) ' ϕ_{im} ' and helium injection technique ' ϕ_{He} .' Petrographically, the studied samples are quartz arenite and ferruginous quartz arenite. The pore types are mostly characterized mostly as (1) intergranular porosity and rarely as (2) intragranular porosity, (3) vuggy porosity, and (4) fracture porosity. The grain elongation ' E ' for the present samples has been measured using the DIA technique; it varies from 1.34 to 1.73. Porosity ' ϕ_{He} ' varies between

25.8 and 34.7 %, gas permeability ' k ' varies from 0.14 to 6.92 μm^2 (very good to excellent rank), and the mean pore diameter ' D ' varies between 3.9 and 25.7 μm (macro to mega pores). The study stated the applicability of the present equation and introduced a number of equations that could be used to calculate porosity, permeability, and pore radius in terms of grain elongation. The applicability of the present study has some limitations due to (1) cementation, (2) microporosity, and (3) fracturing. The effect of cementation can be minimized by processing the grains and the surrounding cement statistically as a bulk ellipsoid unit, whereas the micropores/fractures can be measured by helium injection.

Keywords Porosity · Permeability · Digital Image Analysis · Highly porous Sandstones

Introduction

Different definitions and characterizations have been introduced to describe porosity. Porosity of a given rock is defined as "the percentage of pore spaces in the total volume of the rock," i.e., all the pore spaces not occupied by the solid phase. Porosity is attributed to the fact that at the time of deposition, the clastic components cannot be in continuous form with each other, they are instead are in tangential contact. Grains' shape and orientation play another important role in the grain packing which may be in tangential or straight contact position. Therefore, heterogeneity in pressure distribution, which is carried on relatively small areas of contact between the grains, should be present. This leads to dissolution at the points of contacts and precipitation in the voids (Pettijohn 1984). Moreover, deviatoric stresses can also introduce a crack system enhancing the pore fabric. On the other hand, as a result of cementation, precipitation and infilling of the pore spaces, and other diagenetic changes, the porosity of a sediment is diminished with time and depth (Füchtbauer 1967).

B. S. Nabawy (✉)
Department of Geophysical Sciences,
National Research Center, Dokki,
Cairo, Egypt
e-mail: bsnabawy@yahoo.co.uk

Porosity as the main storage parameter is mainly controlled by primary syn-depositional sedimentary parameters as the grain size, grain shape, sorting, packing, and orientation, whereas controlled by cementation, compaction, dissolution, and recrystallization as post-depositional diagenetic processes.

Porosity is one of the main petrophysical properties of porous reservoir rocks. Therefore, usually, the average output data of a number of measuring techniques are taken into consideration. Sometimes, the most reliable one is taken into consideration.

According to Nabawy et al. (2009), porosity of rock samples has been ranked as (1) negligible ($0 < \emptyset \leq 5\%$), (2) poor ($5 < \emptyset \leq 10\%$), (3) fair ($10 < \emptyset \leq 15\%$), (4) good ($15 < \emptyset \leq 20\%$), (5) very good ($20 < \emptyset \leq 25\%$), and (6) excellent ($25\% < \emptyset$) (modified after Levorsen 1967).

For many decades, classical methods for measuring the grain size/length distribution of sandstones by sieving and studying under polarized microscope (European Committee for Standardization and CEN 1992) have been used. These methods are not very suitable for accurate estimation of the fine sediments (Persson 1998). The reasons for this are the difficulties for fine grains to pass through the sieves and the amount of particles in relation to the sieve area. Furthermore, normal sieve analysis only gives a rough measure of the width of the particles. This does not give all data for a good characterization for the studied sandstones.

In the present study, a simple and cheap technique is applied for characterization of the grain size, shape, and volume of pore spaces using the digital image analysis (DIA). A procedure for using digital image processing techniques was firstly introduced by Berryman (1985) to measure the spatial correlation functions of composite heterogeneous materials.

Porosity of a given rock sample, in general, is recommended to be classified into five types (Fig. 1):

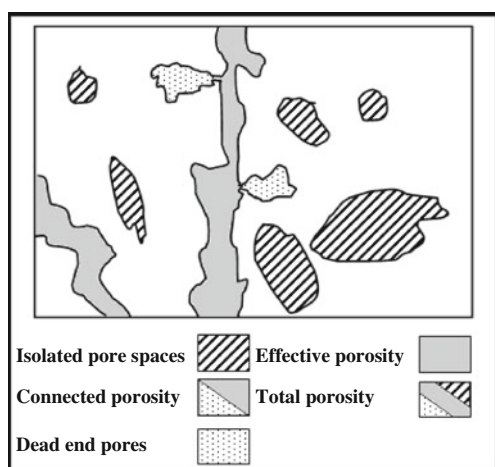


Fig. 1 Schematic illustration showing the main types of porosity

- 1 total porosity (\emptyset_t) consists of all voids within the rock, regardless of whether they are connected or isolated;
- 2 connected porosity (\emptyset_c) is that part of the total porosity which is interconnected together through the pore throats;
- 3 effective porosity (\emptyset_e) is that part of connected porosity which is accessible to free fluids, excluding non-connecting porosity and the volume occupied by the swelled clays (Serra 1984) and hence, is smaller than the connected and total porosity;
- 4 dead-end pore spaces (\emptyset_{Dead}) is that part of the connected porosity which is not accessible for fluids; and
- 5 isolated pore spaces (\emptyset_{iso}) is that part of the total porosity which is isolated away from the fluid path by the cement/matrix. It may be also isolated inside the grains, the crystals, or the fossil remains as intracrystalline, intragranular, or intraparticle.

Where,

$$\emptyset_t = \emptyset_c + \emptyset_{\text{iso}}$$

$$\emptyset_c = \emptyset_e + \emptyset_{\text{Dead}}$$

As a result of cementation, pore filling, dissolution, and other diagenetic changes, porosity may be enhanced or reduced during the geological history, i.e., primary connected porosity will be changed into secondary isolated and dead-end pore spaces. The higher the difference between the total and effective pore spaces reflects the more intensive diagenetic cementation history.

The most important factors enhancing the primary porosity are the grain sorting, roundness, and sphericity as syn-depositional processes, as well as dissolution and leaching out of cement, fracturing, weathering, volume changes, and recrystallization as post-depositional processes enhancing the secondary porosity.

In contrast, primary porosity values are reduced by orientation and packing, whereas cementation, pore filling, authigenic clay minerals, metamorphism, and compaction with depth are reducing factors for both the primary and secondary porosities (Ragab et al. 2000). Pore and grain geometry/fabric (area and elongation) are a key control on other mechanical and physical properties (e.g., permeability, electric and thermal conductivities, magnetic susceptibility, tensile strength, etc.), for example, Lo et al. (1986), Jones and Meredith (1998), Rasolofosaon and Zinszner (2002), Benson (2004), Benson et al. (2005), Louis et al. (2005), Jones et al. (2006), and Nabawy et al. (2009).

Permeability is mostly defined as “the ability of the porous rocks to transmit fluids under certain pressure gradient”; it is measured in millidarcy or micrometers squared.

According to Pettijohn (1984), permeability of consolidated rocks is mostly influenced by (1) the amount of the swelling clays, (2) the ability of the rock to retain the pore water in situ as irreducible water ($S_{w_{irr}}$), (3) channel diameter, (4) wettability, (5) porosity type, and (6) tortuosity and complexity of channels (T). According to Nabawy et al. (2009), porous samples have been classified according to their permeability as (1) fair ($1 < k \leq 10$ md), (2) good ($10 < k \leq 100$ md), (3) very good ($100 < k \leq 1,000$ md), and (4) excellent ($1,000 \text{ md} < k$) (modified after Levorsen 1967).

For the present study, the permeability values will be expressed in micrometers squared; where,

$$\text{md} = 0.9869 \times 10^{-3} \mu\text{m}^2$$

Therefore, the ranks introduced by Nabawy et al. (2009) should be modified to be as follows:

Impermeable	$k \leq 0.0001 \mu\text{m}^2$ (new rank)
Poor	$0.0001 < k \leq 0.001 \mu\text{m}^2$ (new rank)
Fair	$0.001 < k \leq 0.01 \mu\text{m}^2$
Good	$0.01 < k \leq 0.1 \mu\text{m}^2$
Very good	$0.1 < k \leq 1 \mu\text{m}^2$
Excellent	$1 \mu\text{m}^2 < k$

For applicability of the present classification, some approximations are introduced to the limits of the different ranks.

Experimental techniques

A total of 46 highly porous sandstone samples ($\phi_c > 25\%$) were collected from different places in Egypt.

The petrography of the sandstone samples has been studied through a total of 46 thin sections stained by Alizarin Red-S for detecting of dolomite crystals and dyed for porosity studies following Dickson’s technique (1966).

The majority of sandstone classifications are based on texture and/or mineralogy; therefore, microscopic studies are required with accurate determination of the mineral components. The widely used classification of Pettijohn et al. (1973) is used in this study. The nomenclature and classification of porosity were carried out following Choquette and Pray’s classification (1970).

Two types of porosity were determined, the total porosity (ϕ_t) by applying the Digital Image Analysis (DIA) technique and the connected porosity (ϕ_c) by applying the classic fluid injection technique using the Helium Porosimeter.

Porosity (ϕ) and shape anisotropy expressed by grain elongation E^{-1} for the studied sandstone thin sections were measured through two-dimensional petrophysical study using polarized microscope. Two images were taken for each thin section and analyzed using a Leica Qwin 500 Digital Image Analyzer (DIA) in the Image Analyzer

Unit, Pathology Department, National Research Center. The image analyzer was first calibrated automatically to convert the measurement units (pixels) produced by the image analyzer program into actual micrometer units. Ten fields were chosen in each image, and the mean values were obtained.

Processing of the RGB pictures has been started by adjusting the sharpness to the optimum point with no noise obtained for the photographs. The processing was then proceeded by applying median fast filter (4, 4) and fit polynomial filter (2, 2) to enhance the image properties to give up a high-precision photo processing. The photographs were then processed into binary images (black and white), and then, dimensions of grains were measured to define the elongation parameter values for the different grains.

The two-dimensional porosity determination was done by analyzing the particles, and the white areas (grains) were then estimated and related to the total area of the photo. The black areas represent the total pore spaces including the connected and the isolated pore spaces. Comparing the binary image with the original one enables differentiating the total pore spaces into effective, dead-end, and isolated pores. It also enables detecting the presence of some iron pigments which may lead to mistakes in estimating the total pore space area. Differentiating the total pore spaces and eliminating the effect of iron pigments have been done using the cell counter for the cells after adding a grid to the photos (Fig. 4).

The sampled sandstones were then drilled and prepared for the petrophysical measurements as core samples of 25 mm in diameter by 35–50 mm in length. Connected porosity (ϕ) of the dry core-shaped samples was measured using helium injection at 1.2-bar pressure using a gas pycnometer.

The bulk volume and dry weight of 22 selected core samples were measured using a precision caliper (0.01-mm precision) and an electronic balance (0.1-mg precision), whereas the grain volume (v_g) of the samples was measured using the helium pycnometer and the following equation:

$$v_g = 34.989 + \frac{78.899}{1 - (P_1/P_2)}$$

where, P_1 and P_2 are the injection and relaxation pressures, respectively.

Three measurements were carried out for each sample, and the final arithmetic mean was then calculated. The connected porosity (ϕ_{He}) was then calculated using the following equation:

$$\phi_{He} = 100 \times \frac{(v_b - v_g)}{v_b}$$

Permeability was then measured for the selected core samples using a gas permeameter; the core sample was

introduced into a Hasler-type core holder with the outer frame sealed to prevent bypass using pressure of 27.58 bar (400 psi). Dry nitrogen of viscosity μ was injected through the sample at a constant pressure. Taken into consideration the length ' L ', and the cross-sectional area ' A ' of the core samples, the pressure difference between both sides of the sample ' ΔP ', and the flow rate ' Q ,' permeability ' k ' was then calculated using the following equation:

$$k = \frac{Q \times \mu \times L}{A \times \Delta P}$$

The average pore diameter (D) was calculated for the present samples by simulating the pore spaces as pore channel tubes of circular cross-section. Therefore, on the sample scale, the permeability ' k ' of a random network of pore channels of average pore diameter ' D ' and interconnected porosity ' ϕ ' could be assigned as follows (Mavko et al. 2009):

$$D = \sqrt{\frac{32 \times k}{\phi}}$$

Effect of grain size on the intergranular porosity

Fraser (1935) and Graton and Fraser (1935) studied the porosity of six models of spheres packed in six possible arrangements. For the loosest packing and cubic packing, the intergranular porosity was 47.62 %, and for the tightest packing, the porosity was 25.95 %. The present work is a trial to study the effect of the grain size on the intergranular porosity of the cubic loosest packing and the rhombohedral tightest packing models of Graton and Fraser (1935). To study and explain the fact that the finer the grain size, the higher the intergranular porosity, the study were carried out on grains arranged in eight theoretical cubes and rhombohedra models of 20-cm side, the loosest and tightest packing models of Graton and Fraser (1935).

Cubic packing grains (four models)

In the present models, the intergranular porosity was calculated for models of different grain sizes and shapes (Fig. 2; Table 1).

The first two models (Fraser 1935) contain well-rounded spheres in cubic packing with grain size of the first model spheres different from that of the second model spheres. The second two models contain elongated grains arranged in two vertical groups of cubic orientated packing having grain size in the first model different from that in the second model. Each elongated grain is composed of a cylinder and two hemispheres, the diameter of the cylinder equals to that of the accompanied hemispheres.

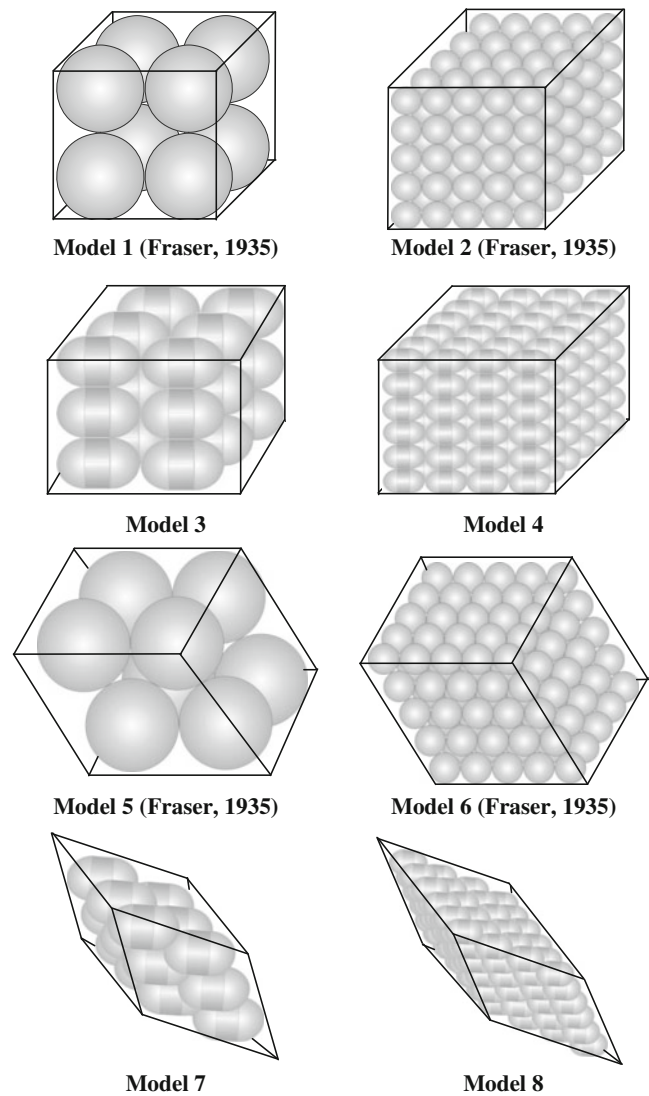


Fig. 2 Eight theoretical models show no effect of grain size on the intergranular porosity within cubic and rhombohedral oriented spherical and elongated grains

The shape anisotropy expressed by grain elongation E^{-1} was calculated using the following equation:

Degree of Elongation (E) = the length of the grain/the diameter of the grain.

Rhombohedral packing grains (four models)

The fifth and sixth models (Fraser 1935) contain well-rounded rhombohedral packed spheres with the same grain sizes of the first and second models, respectively. The seventh and eighth models contain elongated grains arranged in two vertical groups of rhombohedral orientated packing having the same grain sizes of the first and second models, respectively (Fig. 2; Table 1).

Table 1 Number of grains and their shape, elongation, and type of packing for the studied eight models and their intergranular porosity

Model no.	No. grains	Grain shape	Elongation	Packing	∅ %
Cubic packing models					
1	8	Sphere	1	Cubic	47.62
2	125	Sphere	1	Cubic	47.62
3	18	Elongated	1.5	Cubic	38.89
4	144	Elongated	1.5	Cubic	38.89
Rhombohedral packing models					
5	8	Sphere	1	Rhombohedral	25.95
6	125	Sphere	1	Rhombohedral	25.95
7	18	Elongated	1.5	Rhombohedral	13.58
8	144	Elongated	1.5	Rhombohedral	13.58

Effect of grain elongation on the intergranular porosity

In the present study, four models of equi-sized elongated grains in cubic packing have been studied to declare the effect of grain shape/elongation on the intergranular porosity of clastic sediments (Fig. 3; Table 2).

The studied models are represented as cubic models of side length 20 cm. The elongated grains are arranged in two groups vertically in cubic packing, as illustrated in Fig. 3.

Effect of grain sorting on the intergranular porosity

From the statistics of models 1 and 2, it is stated that the grain size of uni-modal well-rounded spheres has no effect on the intergranular porosity of the studied models. On replacement the spheres by uni-modal prolate grains as in models 3 and 4 of the same elongation, it is deduced also that the grain size of the uni-modal prolate grains has no

effect on the total porosity of the studied models. Therefore, the grain size has no effect in both cases.

On adding another group of spheres in models 1 and 2 of the critical size of occupation within the pore spaces, the porosity would be reduced down to 27.07 % in the two cases, i.e., primary porosity will be reduced by 41.05 % of the original value as following:

In model 1, the length of the cube diagonal not occupied by the grains, 14.64 cm, is subdivided into three parts in ratio of 1:2:1 at the corner, the center and the opposite center, respectively. The pore spaces can be occupied with eight spheres of diameter not more than 0.732D (7.32 cm in model 1) as follows:

- 1 The central space of the cube can be occupied by a smaller sphere of diameter 7.32 cm.
- 2 The other three spheres are distributed as six halves at the centers of the faces of the cube.
- 3 Three spheres are distributed as 12 quarters at the centers of the edges of the cube.
- 4 Another sphere is distributed as eight eighths at the corners of the cube.

Therefore, the total pore spaces can be occupied eight spheres of maximum diameter not more than 7.32 cm = 0.732D.

$$\begin{aligned} \text{The volume of the smaller spheres} &= 8 \times \frac{4}{3} \times \pi \times (3.66)^3 \\ &= 1643.6 \text{ cm}^3. \end{aligned}$$

Table 2 Number of grains and their shape/elongation and type of packing for the studied four models and their intergranular porosity

Model no.	No. grains	Elongation	Packing	∅ %
9	32	2	Cubic	34.52
10	72	3	Cubic	30.16
11	200	5	Cubic	26.67
12	800	10	Cubic	24.05

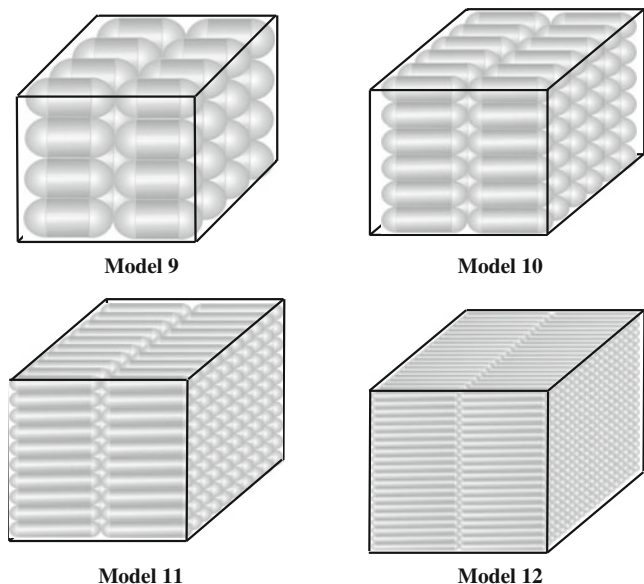


Fig. 3 Theoretical models show the effect of grain elongation on the intergranular porosity between elongated grains

The net porosity = The volume of the not occupied pores /
The volume of the model = $3809.52 - 1643.6 / 8000 = 27.07 \%$

In model 2, the length of the cube diagonal not occupied by the grains is also 14.64 cm subdivided into six parts in the ratio of 1:2:2:2:2:1. The pore spaces can be occupied by grains of maximum diameter not more than $0.732D$ (2.928 cm) as follows:

- 1 The central pore spaces of the cube can be occupied by 64 smaller sphere of diameter 2.928 cm.
- 2 The other 48 spheres are distributed as 96 halves at the centers of the faces of the cube.
- 3 Twelve spheres are distributed as 48 quarters at the centers of the edges of the cube.
- 4 Another sphere is distributed as eight eighths at the corners of the cube.

Therefore, the total pore spaces can be occupied 125 spheres of maximum diameter not more than 2.928 cm.

$$\begin{aligned} \text{The volume of the smaller spheres} &= 125 \times \frac{4}{3} \times \pi \times (1.464)^3 \\ &= 1643.6 \text{ cm}^3. \end{aligned}$$

The net porosity = The volume of the not occupied pores /
The volume of the model = $3809.52 - 1643.6 / 8000 = 27.07 \%$.

Therefore, adding another group of spheres inside the pore spaces in both models 1 and 2 has the same effect regardless the grain size.

On the other hand, the smaller spheres of model 1 (7.32 cm in diameter) cannot be introduced in the pore spaces of model 2 (2.928 cm in diameter), where they are greater than the pore spaces. It is stated that at the same type of sorting and orientation, the smaller the grain size, the smaller the pore diameter; hence, the less ability to receive finer filling reflux and consequently, higher porosity value, and vice versa.

Mineralogical composition

The studied highly porous sandstones are grouped into two main microfacies, quartz arenite and ferruginous quartz arenite.

Quartz arenite

It is composed of fine to very fine angular quartz grains cemented together by silica cement (Fig. 4a). The quartz grains are mostly compacted and cemented together by meniscus cement through point, sometimes suture and

concave–convex contacts. Porosity and grain elongation have been measured using the DIA technique. The pore spaces are represented mainly by (1) intergranular porosity, (2) intragranular porosity, (3) vuggy porosity, sometimes filled with silica cement, and (4) fracture porosity (Fig. 4a, c). Porosity values vary between 37.1 and 43.0 %, i.e., ranked as excellent porosity. The grain elongation varies from 1.42 to 1.73, slightly to moderately elongated (Nabawy et al. 2009) (Table 3).

Ferruginous quartz arenite

The ferruginous quartz arenite is composed of fine to very fine, angular to rounded quartz grains cemented together by gravity silica cement. The quartz grains are mostly compacted together through point, sometimes suture and concave–convex contacts with some quartz grains have wavy extinction. Rare shell remains are noticed (less than 2 %). Many iron oxide patches can be noticed within the cement, and/or iron oxide grains are attached at the surface of the quartz grains and sometimes filling the pore spaces (Fig. 4b).

From the DIA and petrographical study, the pore spaces are represented mainly by (1) intergranular porosity, (2) intragranular porosity, and (3) vuggy porosity sometimes are filled with iron oxides (Fig. 4b, d). Therefore, it is stated that the presence of some iron oxides and clay content filling the pore spaces or disseminated within the cement has negligible effect on the porosity values.

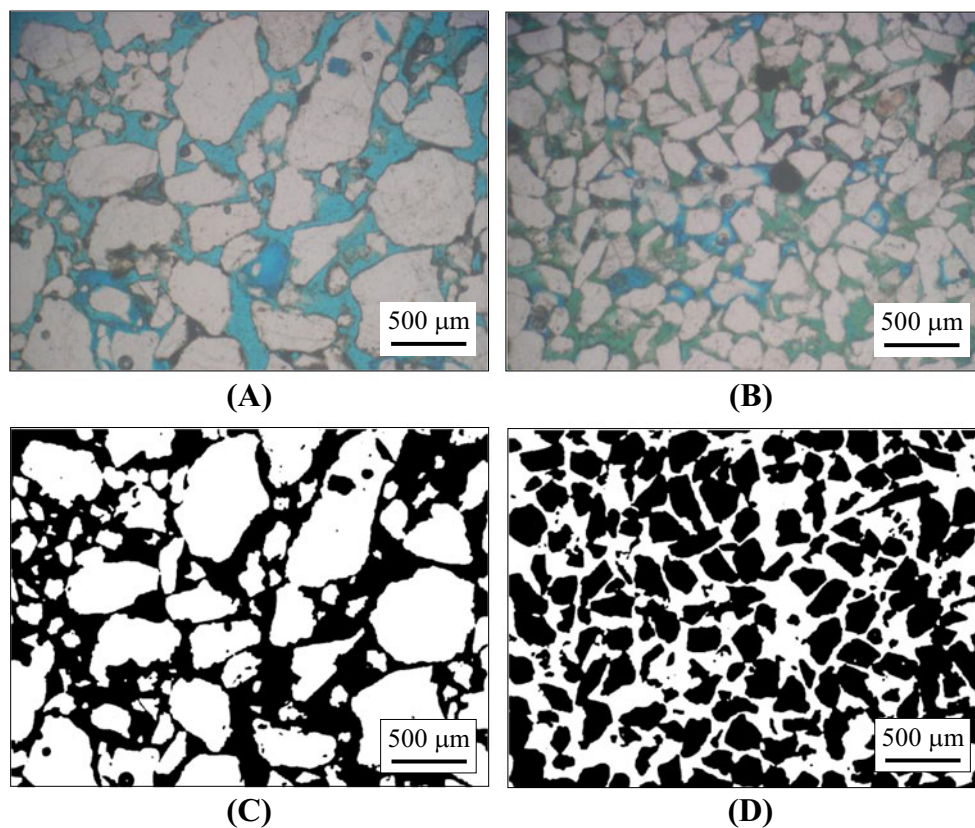
Porosity values vary between 35.3 and 44.4 %, i.e., ranked as excellent porosity. The grain elongation varies from 1.34 to 1.53, slightly elongated (Nabawy et al. 2009) (Table 3).

Results and sample description

Porosity measured using helium injection (ϕ_{He}) varies between 25.8 and 34.7 % ($25 < \phi$, excellent rank; Nabawy et al. 2009) of average 30.1 %, whereas porosity measured by DIA technique (ϕ_{Im}) varies from 35.3 to 44.5 % ($25 < \phi$, excellent rank) of average 40.6 % (Table 3). The bulk and grain densities vary from 1.73 to 2.06 g/cm³ and from 2.62 to 2.79 g/cm³, respectively. The grain elongation factor measured using the digital image analysis (DIA) is relatively low, 1.34 to 1.73 (av. 1.48).

On the other hand, the permeability of the studied highly porous sandstones varies from 0.14 to 6.92 μm^2 of average 2.21 μm^2 ($0.1 \mu\text{m}^2 < k$ up to more than 1 μm^2 , i.e., very good to excellent rank). The mean pore diameter of the present samples varies between 3.9 and 25.7 μm of average 13.2 μm (macro to mega pores).

Fig. 4 Photomicrographs showing; **a** fine to very fine slightly elongated quartz grains cemented together by meniscus cement with excellent intergranular, intragranular, and fracture porosities, PPL; **b** angular to subrounded, fine quartz grains, with some very fine iron oxide grains and patches, PPL; **c** and **d** processed binary black and white images of **a** and **b**, respectively



General discussion

In the present study, it is recommended to discuss the fact stated by Pettijohn (1984) as “the actual size of grains, theoretically, has no influence on porosity, but practically, the fine-grained sediments have a higher porosity than the coarse-grained sediments” should be explained and modified. The present study reveals that “the higher the grain size, the higher the pore diameter, hence the higher the ability of the pore space to receive finer filling reflux.”

The post deposition, the diameter of pore throats, and tortuosity of channel porosity are other main factors, must be taken into consideration in practice, control receiving the sedimentary reflux.

From the studied models, the shape/elongation of the grains as anisotropy parameter, whether they are spherical grains (isotropic grains) or elongated ones (anisotropic grains) and its degree of elongation (*E*) have an observed effect on the present intergranular porosity.

From the statistical analysis, total porosity values (ϕ_t) in the cubic packing models of the spheres and elongated grains (models 1, 4, 9–12) are directly related to the degree of elongation (*E*) with the maximum correlation coefficient (Fig. 5) by the following equation:

$$\phi = 26.188 E^{-1} + 21.431 \quad (r = 1.00)$$

In the studied models 3, 4, and 9 to 12, the total pore spaces between the *terminals of the prolate grains* can be occupied syn-depositionally by spheres of maximum diameter 0.732 times the diameter of the elongated grains (*D*) and post-depositionally by spheres of maximum diameter = $(D \sqrt{2} - D) = D (\sqrt{2} - 1) = 0.414 D$.

On the other hand, the pore spaces between the *body of the prolate grains* can be occupied syn-depositionally or post-depositionally by spheres of maximum diameter = $0.414D$

On rhombohedral orientation, the maximum diameter of grains which can be received post-depositionally = $\frac{(D\sqrt{3}-D)}{6} = D \frac{(\sqrt{3}-1)}{6} = 0.122D$.

In general, the calculated porosity for the studied models is based on well-rounded spheres and on cylinders of well-rounded cross-section and terminals; otherwise, the porosity will be much greater than the calculated values. The scratched surface of the grains and its irregularity greatly decrease the maximum possible diameter of the received grains. Well cementation may reduce the net porosity down to negligible values.

A further extension for this study is recommended by replacing the prolate grains by bladed and oblate grains in a study for investigating the effect of the degree of blading and oblateness on the interstitial pore spaces.

Table 3 Petrographical, DIA, and petrophysical values of the studied highly porous sandstones

S. no.	σ_b	σ_g	ϕ_{He}	k	D	ϕ_{Im}	E	E^{-1}
1	1.83	2.65	30.9	2.81	17.1	39.7	1.48	0.68
2	1.98	2.74	27.7	0.38	6.70	37.1	1.63	0.61
4	2.06	2.79	26.2	0.26	5.60	36.3	1.73	0.58
5	1.74	2.63	33.8	4.35	20.3	43.9	1.38	0.72
6	1.75	2.63	33.5	6.92	25.7	43.0	1.34	0.75
7	1.88	2.62	28.2	0.61	7.81	39.7	1.60	0.63
9	1.92	2.64	27.3	0.64	8.46	38.8	1.56	0.64
11	1.73	2.65	34.7	2.70	15.8	43.4	1.35	0.74
13	1.77	2.65	33.2	2.44	15.3	43.2	1.40	0.71
14	1.94	2.64	26.5	0.58	8.38	39.9	1.61	0.62
20	1.87	2.67	30.0	–	–	42.5	1.46	0.68
22	1.90	2.67	28.8	0.14	3.91	39.8	1.57	0.64
23	1.73	2.64	34.5	–	–	44.4	1.34	0.75
25	1.78	2.64	32.6	1.68	12.9	44.2	1.38	0.72
26	1.83	2.64	30.7	4.35	21.4	38.2	1.42	0.70
28	1.84	2.64	30.3	4.43	21.6	43.3	1.43	0.70
30	1.96	2.64	25.8	–	–	38.1	1.57	0.64
34	1.92	2.63	27.0	–	–	39.9	1.52	0.66
37	1.89	2.65	28.7	1.24	11.8	35.7	1.47	0.68
39	1.87	2.64	29.2	0.32	5.92	42.3	1.50	0.67
40	1.83	2.65	30.9	1.15	10.9	40.7	1.42	0.70
44	1.77	2.70	34.4	–	–	44.5	1.35	0.74
46	1.91	2.63	27.4	–	–	35.3	1.53	0.65

σ_b and σ_g (g/cm³) are the bulk and grain densities, respectively; ϕ_{He} and ϕ_{Im} (percent) are the porosity values measured by helium injection and DIA techniques, respectively; k (μm^2) is the measured gas permeability; D (μm) is the calculated pore diameter; E and E^{-1} are the grain elongation and its reciprocal, respectively

According to Pettijohn (1984), these theoretical concepts cannot be applied too literally to natural deposits because the latter neither composed of spheres/elongated grains nor packed in a wholly systematic manner. Therefore, the

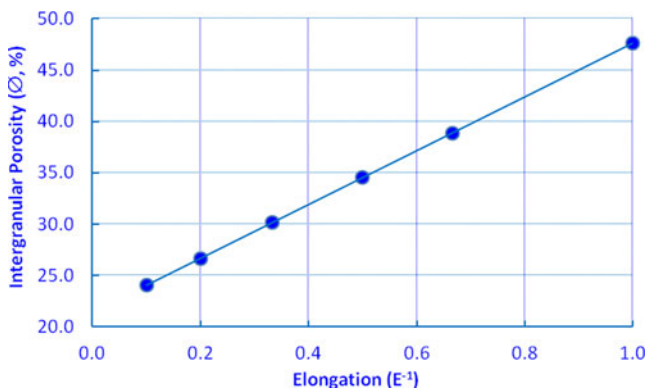


Fig. 5 The relation between the grain elongation values and the intergranular porosity for the studied cubic models

present study could be considered as a preliminary study for further studies on different grain shapes of the clastic rocks.

On contrary with that mentioned by Pettijohn (1984), it is thought that the present theoretical concept is applicable for the highly porous sandstones of primary intergranular porosity. Hence, the more intensive diagenetic history means more limitations to the reliability of the present concept. The ideal relationship between the elongation of the grains and the total porosity should be limited by (1) cementation, (2) microporosity, and (3) fracturing. The effect of cementation can be minimized by processing the grains and the surrounding cement statistically as a bulk ellipsoid unit, whereas the effects of microporosity and fractures can be minimized by measuring porosity using helium injection.

In the following paragraph, the proposed theoretical equation has been applied to the studied highly porous sandstone samples. The digital image analysis technique was successful for measuring the grain elongation factor (E) and the intergranular porosity (ϕ_{Im}). The measured mean grain elongation for the different samples has been plotted against the calculated and the measured porosity, as in Fig. 6.

$$\phi_{Im} = 45.73 E^{-1} + 9.19 \quad (r = 0.92)$$

Helium gas injection technique has the ability to invade into the micropores and fractures which cannot be estimated using the image analysis with good accuracy. Hence, to minimize the limitation caused by the microporosity and fractures, porosity has been measured using helium injection. The helium porosity is highly correlated ($r=0.80$) with that measured using image analysis (Fig. 7).

$$\phi_{Im} = 0.80 \phi_{He} + 16.5 \quad (r = 0.80)$$

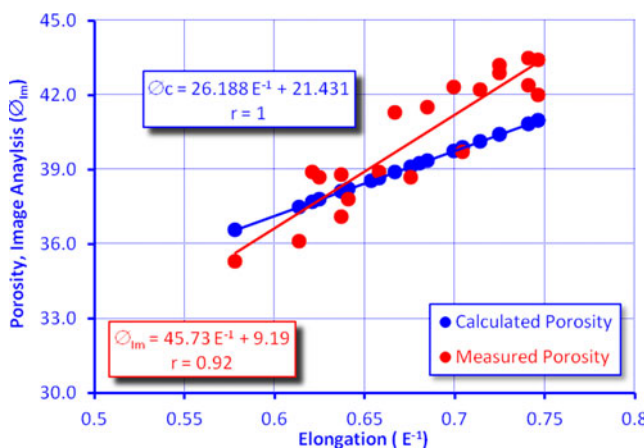


Fig. 6 Plotting the measured and calculated porosity versus the measured elongation degree

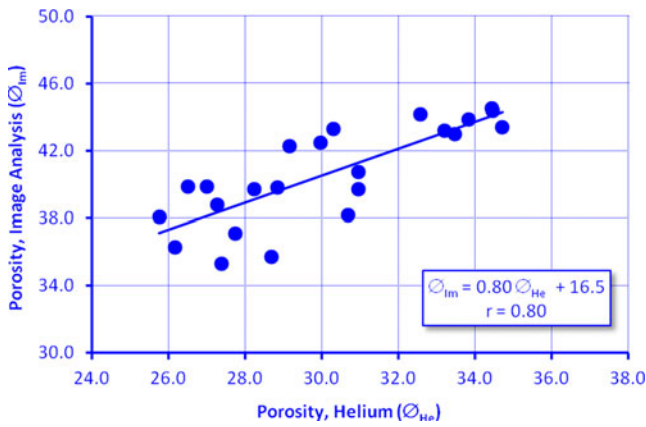


Fig. 7 Plotting porosity measured by helium injection technique versus that measured by Digital Image Analysis technique

In addition to the ability of the helium to invade into the micropores, measuring porosity using the helium injection is a fast and easy method saving time consumed during measuring porosity by image analysis method. The helium porosity of the present samples was plotted versus the elongation degree (Fig. 8) with the same reliability of the porosity measured using image analysis. It is calculated in terms of the elongation degree using the following equation:

$$\phi_{He} = 56.12 E^{-1} - 8.00 \quad (r = 0.92)$$

Gas permeability has been measured also for the same samples, and the results were plotted versus the obtained elongation degree in an exponential relationship with good reliability (Fig. 9)

$$k = 206.3 E^{-13.11} \quad (r = 0.82)$$

The shape and elongation of the pore spaces are a direct and logic impact of shape and elongation of the grains forming and surrounding the pores. Therefore, the reliable relationship between the gas permeability and the grain elongation can be related to the effect of the grain elongation

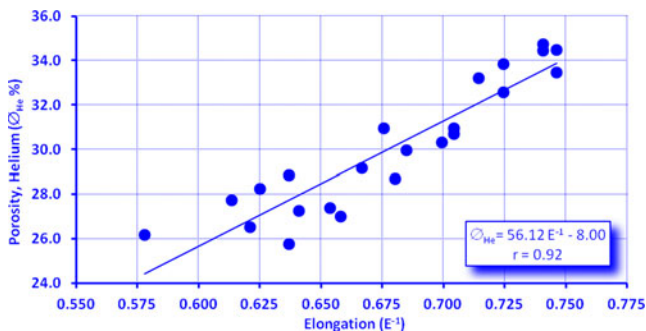


Fig. 8 Plotting helium porosity (ϕ_{He}) versus grain elongation degree (E) measured using the image analysis technique

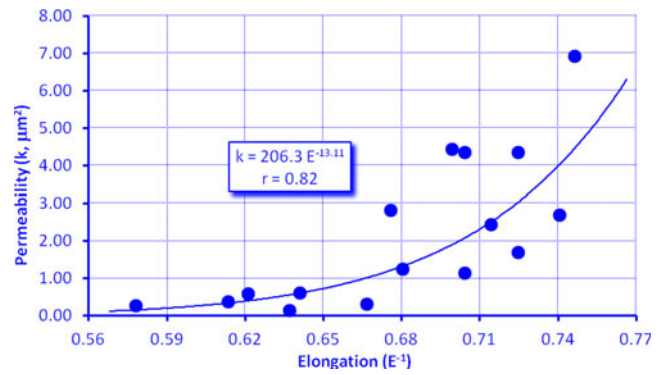


Fig. 9 Plotting gas permeability (k) versus grain elongation degree (E) measured using the image analysis technique

and the total porosity on the shape and diameter of the interstitial pore spaces. Also, it was expected to get a good relationship between the grain elongation and the pore diameter (D).

The mean pore diameter (D) of the present samples is related to the grain elongation in a good exponential relationship (Fig. 10) and can be calculated in terms of the pore elongation using the following equation:

$$D = 119.0 E^{-5.99} \quad (r = 0.80)$$

In general, the proposed models and the obtained physical equation relating the grain elongation to the intergranular pore volume are applicable to the highly porous sandstones. Using the proposed equation as well as the other introduced empirical equations, it is possible to calculate the intergranular porosity, permeability, and the average pore diameter.

Applying the multiregression analysis for the present grain elongation, porosity, and permeability values indicates the ability to calculate the elongation factor in terms of porosity and permeability using the following equation:

$$E^{-1} = 0.015 \phi_{He} + 0.005 k + 0.229 \quad (r = 0.94)$$

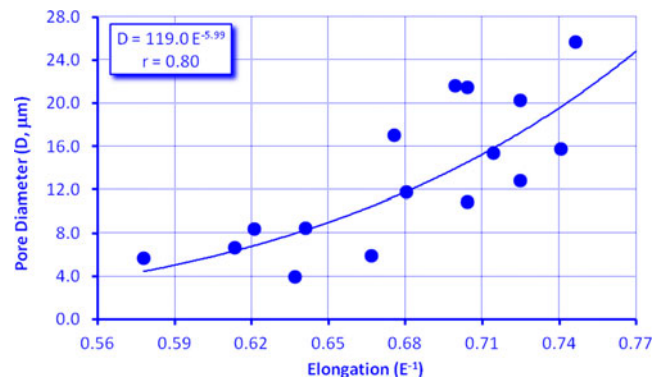


Fig. 10 Plotting the pore diameter (D) in micrometers versus elongation degree (E) measured using the image analysis technique

Conclusions

The present study reveals that the grain size has no effect on the intergranular porosity, but the higher the grain size, the higher the interstitial pore diameter; therefore, the higher ability to receive finer filling reflux and then the lower porosity value. The effect of the grain elongation, as a shape anisotropy parameter, on the interstitial pore volume has been also discussed using eight theoretical models. A new equation has been introduced relating the elongation factor (E), measured by DIA technique, to the pore volume measured by helium injection and DIA techniques. Consequently, it is concluded that the petrophysical parameters of the present samples, represented by porosity, permeability, and pore diameter, are mostly controlled by the grain shape anisotropy represented by the grain elongation ' E '.

Other equations relating the gas permeability and pore diameter to the elongation factor (E) 'anisotropy parameter' are also introduced with high reliability. The introduced equations are applicable to the highly porous sandstones. Cementation, matrix porosity, and fractures are limitations for using the present equations. These limitations have been overcome using DIA technique by processing the cemented grains as bulk ellipsoids, whereas the micropores/fractures have been overcome by measuring porosity using helium injection technique.

Recommendation

The present study is based on the main assumption that the grain orientation is geometrically systematic along one long axis of elongation which seems to be natural and more accepted; it is usually caused by flowing depositional currents and load pressure. However, spatial dispersion of the grain orientation may present. This spatial random orientation has a great crucial effect on permeability and electric conductivity. Further studies are planned to study the spatial distribution of grain orientation and its effect on different conductivity parameters.

Acknowledgments I would like to thank the reviewers for their great comments that improved and reconstructed the manuscript. I would also like to give thanks to Editor Prof Abdullah M. Al-Amri whose patience and insightful suggestions have led to a new concise revised version.

References

- Benson PM (2004) Experimental study of void space, permeability and elastic anisotropy in crustal rock under ambient and hydrostatic pressure, Ph.D. thesis. University of London, London
- Benson PM, Meredith PG, Platzman ES, White RE (2005) Pore fabric shape anisotropy in porous sandstone and its relation to elastic and permeability anisotropy under isostatic pressure. *Int J Rock Mech* 42:890–899
- Berryman JG (1985) Measurement of spatial correlation functions using image processing techniques. *J Appl Physics* 57(7):2374–2384
- Choquette PW, Pray LC (1970) Geologic nomenclature and classification of porosity in sedimentary carbonates. *Bull Am Ass Petrol Geol* 54(2):207–250
- Dickson JAD (1966) Carbonate identification and genesis revealed by staining. *J Sediment Petrol* 36(2):491–505
- European Committee for Standardization, CEN, (1992) European Standard Program EN 993–1 (Proposed Draft); Tests for geometrical properties of aggregates, Part 1: Determination of particle size distribution granulometric analysis (sieving Method). CEN Brussels.
- Fraser HJ (1935) Experimental study of the porosity and permeability of clastic sediments. *J Geology* 43:910–1010
- Füchtbauer H (1967) Influence of different types of diagenesis on sandstone porosity. *Proc. 7th World Petrol. Cong Mexico* 2:353–369
- Graton LC, Fraser HJ (1935) Systematic packing of spheres, with particular relation to porosity and permeability. *J Geology* 43:785–909
- Jones C, Meredith PG (1998) An experimental study of elastic wave propagation anisotropy and permeability anisotropy in an illitic shale, in Eurock'98. *Rock Mech Petrol Eng* 2:307–313
- Jones S, Benson P, Meredith P (2006) Pore fabric anisotropy: testing the equivalent pore concept using magnetic measurements on synthetic voids of known geometry. *Geophys J Int* 66:485–492
- Levorsen AI (1967) *Geology of Petroleum*. W.H. Freeman Company, San Francisco, USA
- Lo TW, Coyner KB, Toksoz MN (1986) Experimental determination of elastic anisotropy of Berea sandstone, Chicopee shale, and Chelmsford granite. *Geophysics* 51:164–171
- Louis L, David C, Metz V, Robion P, Menendez B, Kissel C (2005) Microstructural control on the anisotropy of elastic and transport properties in undeformed sandstones. *Int J Rock Mech* 42:911–923
- Mavko G, Mukerji T, Dvorkin J (2009) *The rock physics handbook: tools for seismic analysis of porous media*, 2nd edn. Cambridge Univ, Press, England
- Nabawy BS, Rochette P, Géraud Y (2009) Petrophysical and magnetic pore network anisotropy of some cretaceous sandstone from Tushka Basin, Egypt. *Geophys J Int* 177(1):43–61
- Persson AL (1998) Image analysis of shape and size of fine aggregates. *J Eng Geology* 50(1–2):177–186
- Pettijohn EJ (1984) *Sedimentary rocks*, 3rd edn. CBS publishers & Distributors, Delhi
- Pettijohn FJ, Potter PE, Siever R (1973) *Sand and Sandstone*. Springer-Verlag, Berlin, p 618
- Ragab MA, El Sayed AA, Nabawy BS (2000) In: Soliman SM (ed) *Physical parameters of Egyptian oil reservoir sedimentary rocks: a review*, in *Sedimentary Geology of Egypt: applications and economics*. Sedimentological society of Egypt, Cairo, pp 129–150
- Rasolofosaon PNJ, Zinszner BE (2002) Comparison between permeability anisotropy and elastic anisotropy of reservoir rocks. *Geophysics* 67:230–240
- Serra O (1984) *Fundamentals of well-log interpretation*. Elsevier, Amsterdam